BIOCHEMISTRY
including biophysical chemistry & molecular biology
Article

Biochemistry **2010,** *49,* 1033–1041 1033
DOI: 10.1021/bi901780j

Structural and Kinetic Characterization of the LPS Biosynthetic Enzyme D-α,β-D-Heptose-1,7-bisphosphate Phosphatase (GmhB) from *Escherichia coli*[†,‡]

Patricia L. Taylor,[§] Seiji Sugiman-Marangos,[§] Kun Zhang,[§] Miguel A. Valvano,[∥] Gerard D. Wright,[§] and Murray S. Junop*[,§]

[§]*Department of Biochemistry and Biomedical Sciences and M. G. DeGroote Institute for Infectious Disease Research, McMaster University, 1200 Main Street West, Hamilton, Ontario L8N 3Z5, Canada and* [∥]*Infectious Diseases Research Group, Siebens Drake Research Institute, Department of Microbiology and Immunology, University of Western Ontario, London, Ontario N6A 5C1, Canada*

Received October 15, 2009; Revised Manuscript Received January 5, 2010

ABSTRACT: Lipopolysaccharide is a major component of the outer membrane of Gram-negative bacteria and provides a permeability barrier to many commonly used antibiotics. ADP-heptose residues are an integral part of the LPS inner core, and mutants deficient in heptose biosynthesis demonstrate increased membrane permeability. The heptose biosynthesis pathway involves phosphorylation and dephosphorylation steps not found in other pathways for the synthesis of nucleotide sugar precursors. Consequently, the heptose biosynthetic pathway has been marked as a novel target for antibiotic adjuvants, which are compounds that facilitate and potentiate antibiotic activity. D-α,β-D-Heptose-1,7-bisphosphate phosphatase (GmhB) catalyzes the third essential step of LPS heptose biosynthesis. This study describes the first crystal structure of GmhB and enzymatic analysis of the protein. Structure-guided mutations followed by steady state kinetic analysis, together with established precedent for HAD phosphatases, suggest that GmhB functions through a phosphoaspartate intermediate. This study provides insight into the structure−function relationship of GmhB, a new target for combatting Gram-negative bacterial infection.

The development of antimicrobial agents in the 20th century has resulted in dramatic declines in the number of deaths from infectious disease. The resulting widespread use and misuse of these drugs has provided selective pressure for the emergence of bacteria that are resistant to many commonly used antibiotics. In particular, Gram-negative pathogens resistant to most, if not all, currently available drugs are proving to be especially concerning.

The Gram-negative outer membrane (OM)[1] provides a potent barrier to many drugs and is also essential for cell viability. OM drug targets, such as lipopolysaccharide (LPS) biosynthesis enzymes, are currently being explored for use to combat infection caused by Gram-negative pathogens. The outer membrane is an especially attractive target given the large arsenal of antibiotics clinically available for treating Gram-positive bacteria, which are ineffective against Gram-negative bacteria because of low permeability. Agents that could increase the permeability of the Gram-negative OM to such antibiotics may likely be advantageous for combination therapies with otherwise excluded antibiotics (*1*−*3*).

The OM is an asymmetric bilayer consisting of an inner leaflet rich in phospholipids and an LPS-rich outer leaflet. The LPS component provides an effective permeability barrier to small, hydrophobic molecules. LPS typically consists of three major components: (1) lipid A and inner core oligosaccharide (OS), consisting of 2-keto-3-deoxy-D-*manno*-octulosonic acid (Kdo) and one or more L-*glycero*-D-*manno*-heptose residues; (2) an outer core OS made of various linked sugar residues; and (3) O antigen polysaccharide chains of variable length and composition (reviewed in refs *2* and *4*−*6*). The lipid A-Kdo domain is highly conserved among most Gram-negative bacteria and is the minimum LPS structure required for the maintenance of OM integrity for bacterial survival. Thus, several lipid A-Kdo biosynthetic steps are essential to bacterial growth and proven targets for antibiotics (*7*, *8*). The outer core OS and O antigen are not essential for bacterial growth, but they mediate host−microbe interactions and contribute significantly to virulence and permeability of the OM to small molecules such as antibiotics (*4*).

It is widely accepted that the strength of the diffusion barrier is due to the high level of packing of the acylated lipid A and lateral interactions of individual LPS molecules (*9*). Phosphorylated heptose molecules in the inner core OS bind divalent cations, cross-linking the LPS and further decreasing the permeability of the OM. Mutants in heptose biosynthesis lack this cross-linking capability, and while capable of survival in a laboratory setting, they display markedly reduced antibiotic resistance and pathogenicity (*10*, *11*). The biosynthetic pathway of the L-*glycero*-D-*manno*-heptose molecule in Gram-negative bacteria has been elucidated and is illustrated in Figure 1 (*12*, *13*). When we started

[†]This work was supported by a Canadian Institutes of Health Research Operating Grant (XNE-8705) to G.D.W., M.A.V., and M.S.J. and fellowships from the National Science and Research Council of Canada (S.S.-M.) and Canadian Cystic Fibrosis Foundation (P.L.T.).

[‡]The structure factor amplitudes and the refined coordinates of apo-GmhB, GmhB·Ca, and GmhB·Ca·P structures have been deposited in the Protein Data Bank as entries 2GMW, 3L1U, and 3L1V, respectively.

*To whom correspondence should be addressed: Department of Biochemistry and Biomedical Sciences, 1200 Main St. W., Health Sciences Center Room 4N20A, Hamilton, Ontario L8N 3Z5, Canada. Phone: (905) 525-9140, ext. 22912. Fax: (905) 522-9033. E-mail: junopm@mcmaster.ca.

[1]Abbreviations: HAD, haloacid dehydrogenase; HBP, D-*glycero*-D-*manno*-heptose 1,7-bisphosphate; HEPES, 4-(2-hydroxyethyl)-1-piperazineethanesulfonic acid; IPTG, isopropyl β-D-1-thiogalactopyranoside; Kdo, 2-keto-3-deoxy-D-*manno*-octulosonic acid; LPS, lipopolysaccharide; MIC, minimum inhibitory concentration; OM, outer membrane; OS, oligosaccharide; PDB, Protein Data Bank; rmsd, root-mean-square deviation; S7P, sedoheptulose 7-phosphate; SeMet, selenomethionine.

Published on Web 01/05/2010

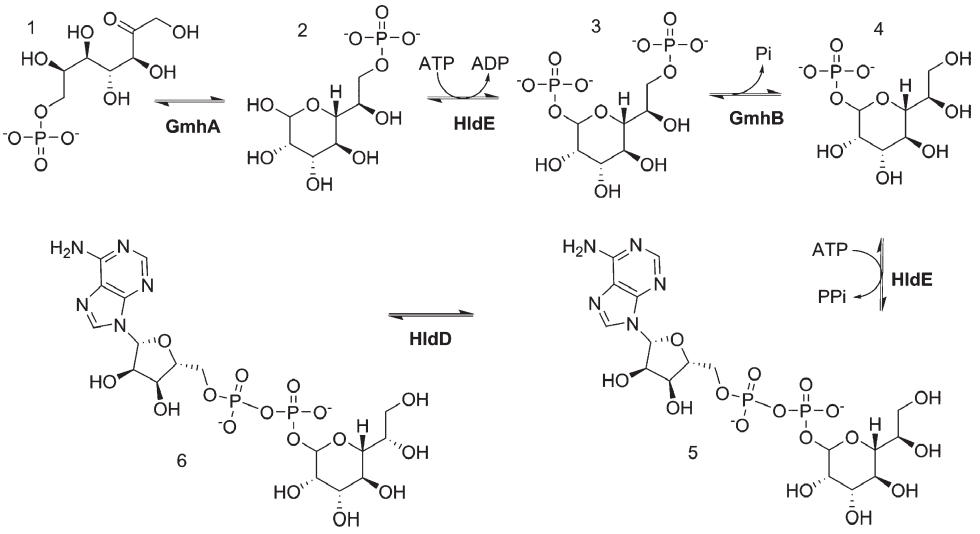

FIGURE 1: Schematic of the ADP-L-*glycero*-D-*manno*-heptose biosynthetic pathway: (1) sedoheptulose 7-phosphate, (2) D-*glycero*-D-*manno*-heptose 7-phosphate, (3) D-*glycero*-D-*manno*-heptose 1,7-bisphosphate, (4) D-*glycero*-D-*manno*-heptose 1-phosphate, (5) ADP-D-*glycero*-D-*manno*-heptose, and (6) ADP-L-*glycero*-D-*manno*-heptose.

from sedoheptulose 7-phosphate (S7P), sedoheptulose-7-phosphate isomerase (GmhA) is the first committed enzyme in the pathway (*14*−*16*). In *Escherichia coli*, phosphorylation at the 1 position of the resulting D-*glycero*-D-*manno*-heptose 7-phosphate is then catalyzed by the kinase moiety of the bifunctional D-*β*-D-heptose phosphate kinase/D-*β*-D-heptose-1-phosphate adenyltransferase (HldE) (*9*, *17*). A bifunctional HldE is present in bacteria such as *E. coli* and *Pseudomonas aeruginosa* on the basis of genomic sequence comparison. However, in some organisms such as *Burkholderia cenocepacia*, a significant pathogen in cystic fibrosis patients, this bifunctional enzyme is replaced by two distinct enzymes, HldA and HldC, which accomplish the respective functions (*18*). D-α,*β*-D-Heptose-1,7-bisphosphate phosphatase (GmhB) catalyzes the removal of the phosphate at the 7 position (*12*) (*13*), while the adenyltransferase action of HldE (or HldC) transfers the AMP moiety from ATP, giving rise to ADP-D-*glycero*-D-*manno*-heptose. Finally, ADP-D-*β*-D-heptose epimerase (HldE) catalyzes the formation of ADP-L-*glycero*-D-*manno*-heptose, the precursor to the final LPS heptose molecule (*19*, *20*). This study focuses on GmhB, which performs the third conserved step in the ADP-heptose biosynthesis pathway.

Primary amino acid sequence analysis of GmhB has classified the protein within the haloacid dehydrogenase (HAD) family of hydrolyases, part of the large DDDD superfamily of phosphohydrolases, in which phosphatases are a small portion (*11*). Members of this family, such as histidinol-phosphate phosphatase (HisB) (*21*) and *β*-phosphoglucomutase (*22*), have characteristic conserved motifs: motif I, DXDX(T/V), where the first aspartic acid is the attacking nucleophile on the substrate phosphate group and the second protonates the dephosphorylated leaving group; motif II, S/T, involved in binding the substrate phosphate; and motif III, (G/S)DXX(N/T)D, which comprises the remainder of the active site to orient the substrate and bind the catalytic divalent cation (Mg^{2+}). The catalytic aspartate, an invariant residue, makes use of the metal ion to attack the phosphorus of the substrate, resulting in cleavage of the phosphoester bond and formation of a phosphoaspartate intermediate. An activated water molecule then attacks the phosphoaspartate, releasing inorganic phosphate (*22*−*24*). In this paper, we report for the first time the three-dimensional (3D) structure of GmhB and demonstrate by enzymatic and mutational analyses that GmhB is a member of the HAD family of phosphohydrolases.

EXPERIMENTAL PROCEDURES

Expression Plasmids. The IPTG inducible pET28a(+) (Novagen) plasmid pET28a(+)*gmhB*, encoding the *E. coli* GmhB with an N-terminal hexahistidine tag (*25*), was used for *in vitro* studies. The insert in pET28a(+)*gmhB* was excised between the *Xba*I and *Hin*dIII sites, purified by agarose gel electrophoresis, and ligated at these sites into a low-copy number pBAD30 arabinose-inducible vector. The ligation reaction was conducted overnight at 16 °C using T4 DNA ligase (New England Biolabs) according to the manufacturer's protocol. The resulting plasmid, pBAD30*gmhB*, was used for *in vivo* studies.

Expression Strains. *E. coli* BL21(DE3) [F^- *ompT gal dcm lon hsdS*$_B$(r_B^- m_B^-) *λ* [DE3: *lacI lac*UV5-T7 gene 1 *ind1 sam7 nin5*]] bacteria were transformed with pET28a(+)*gmhB* parental and mutant plasmids and used to overexpress these proteins for purification. A *gmhB* deletion strain (BW25113Δ*gmhB*) was generated via replacement of the *gmhB* gene with a kanamycin resistance gene (Kan^R) in *E. coli* BW25113 (*lacI*^{q} *rrnB*$_{T14}$ Δ*lacZ*$_{WJ16}$ *hsdR514* Δ*araBA-D*$_{AH33}$ Δ*rhaBAD*$_{LD78}$), using the protocol described by Datsenko et al. (*26*). Specific primers were designed with regions homologous to both the Kan^R from source vector pKD4 and the chromosomal *gmhB*: forward, 5′ CGATACTAGCGTCACATGCCTTATTAAGGAGCTATAAAAGGTGTAGGCTGGAGCTGCTTC 3′; reverse, 5′ AGCGGAAAAATGCATTTTTATTTCAACCGCTCATCTTTTAACATATGAATATCCTCCTTA 3′. Kan^R was amplified from pKD4 using these dual primers by PCR, digested with *Dpn*I, and used to transform electrocompetent *E. coli* BW25113 pKD46. Transformants were grown sequentially on LB agar with 15 *μ*g/mL kanamycin (overnight at 37 °C), LB agar (43 °C, 2 h), and LB agar with 50 *μ*g/mL kanamycin (overnight at 37 °C). Loss of helper plasmid pKD46 was confirmed by lack of growth on LB agar with 100 *μ*g/mL ampicillin at 37 °C overnight.

Mutagenesis. Site-directed mutations were generated in pET28a(+)*gmhB* using QuikChange site-directed mutagenesis (Stratagene), according to the manufacturer's protocol.

Table 1: GmhB Data Collection and Model Refinement Statistics

	apo (SeMet)	apo (native)	calcium-bound	calcium- and phosphate-bound
		Data Collection		
space group	$P2_12_12_1$	$P2_12_12_1$	$P2_12_12_1$	$P2_12_12_1$
cell parameters				
a, b, c (Å)	52.00, 64.87, 103.39	51.90, 63.98, 103.32	50.58, 63.91, 105.35	50.35, 64.19, 103.67
α, β, γ (deg)	90, 90, 90	90, 90, 90	90, 90, 90	90, 90, 90
no. of molecules per asymmetric	2	2	2	2
resolution[a,b] (Å)	46.46−1.85 (1.92−1.85)	40.19−1.50 (1.55−1.50)	45.59−1.95 (2.02−1.95)	45.29−1.95 (2.02−1.95)
no. of unique reflections	57709	54729	25327	24747
redundancy[a]	7.17 (7.06)	5.47 (3.34)	4.03 (3.91)	3.89 (3.89)
completeness[a] (%)	100.0 (100.0)	99.8 (93.1)	99.0 (98.8)	98.3 (100.0)
$I/\sigma(I)$[a]	16.8 (4.9)	22.7 (4.4)	9.2 (3.4)	6.6 (2.6)
R_{merge}[a] (%)	5.6 (36.3)	3.1 (25.3)	6.2 (33.1)	11.0 (42.6)
		Model and Refinement		
resolution[a] (Å)		25.00−1.50	45.57−1.95	27.135−1.95
R_{work}/R_{free} (%)		16.0/21.0	23.4/25.7	24.9/28.4
no. of observed reflections		51887	24872	23855
no. of free reflections		2761	1965	1928
no. of atoms				
protein		3048	2848	2830
ligand/ion		2	4	14
water		567	345	251
root-mean-square deviation				
bond lengths (Å)		0.010	0.006	0.014
bond angles (deg)		1.380	1.012	1.36
mean B factor (Å^2)		23.26	29.93	32.84
estimated coordinate error (Å)		0.06	0.12	0.12
PDB entry		2GMW	3L1U	3L1V

[a]Statistics for the highest-resolution shell are shown in parentheses. [b]Data cutoff $F > 0$.

Site-directed mutants and their corresponding primers are described in Table S1 of the Supporting Information. Mutations were verified by plasmid DNA sequence analysis (MOBIX, McMaster University) using vector specific sequencing primers (Table S1).

GmhB Protein Purification. Parental and mutant hexahistidine-tagged GmhB proteins were overexpressed and purified from their respective *E. coli* BL21(DE3) pET28a(+)*gmhB* strains by immobilized metal affinity chromatography using a 5 mL Ni-NTA chelating column (Qiagen) and an imidazole gradient [GmhB buffer A which consists of 50 mM HEPES (pH 8.0) and 20 mM imidazole; GmhB buffer B which consists of 50 mM HEPES (pH 8.0) and 250 mM imidazole], as previously described (*25*). Fractions containing purified protein were verified using SDS−15% polyacrylamide gel electrophoresis, combined, dialyzed overnight in 20 mM HEPES (pH 8.0), and concentrated using Amicon 5 Ultra centrifugation filters (Millipore). The protein concentration was determined with the Bradford assay, and proteins were stored at −20 °C in 50% (v/v) glycerol. Selenomethionine (SeMet)-labeled GmhB for SAD phasing was prepared using a previously described method (*27*) and purified as described above . Prior to crystallization, protein was dialyzed overnight in buffer containing 20 mM HEPES (pH 8.0) and 3% (v/v) 2-propanol.

Determination of the 3D Structure of GmhB. GmhB crystals were all grown at 20 °C using the hanging-drop vapor diffusion method. Native GmhB (9.6 mg/mL) was mixed in a ratio of 1 μL to 1 μL with crystallization solution [25% (w/v) polyethylene glycol (PEG) 3350, 0.1 M Tris (pH 8.5), and 0.02 M sodium chloride] and equilibrated against 0.5 mL of crystallization solution. GmhB-SeMet (3.8 mg/mL) was mixed in a ratio of 4 μL to 2 μL with crystallization solution [25% (w/v) PEG 3350, 0.1 M Tris (pH 7.8), 0.005 M DTT, 0.025 M sodium chloride, and 11% (v/v) glycerol] and 0.6 μL of 0.018 M *N*-dodecyl β-D-maltoside and equilibrated against 0.5 mL of crystallization solution. Cocrystals of calcium-bound GmhB or calcium- and phosphate-bound GmhB were obtained by overnight soaking of native GmhB crystals in either 0.005 M calcium chloride or 0.005 M calcium chloride with 0.005 M sodium phosphate, respectively.

Native and SeMet apo data sets were collected at wavelengths of 1.1 and 0.979 Å on X8C and X12C beamlines, respectively, of the National Synchrotron Light Source at Brookhaven National Laboratory (Upton, NY). Data sets were processed and scaled with d*TREK (*28*) to 1.5 and 1.85 Å, respectively. All 16 of the expected SeMet sites were located using HYSS (*28*, *29*). Phasing and density modification conducted with CNS was used to generate an experimental map. CNS (*30*) and Coot (*31*) were used to build an initial model using the SeMet data. This model was then refined against the higher-resolution native data set (*32*). Calcium-bound and calcium- and phosphate-bound data sets were collected at a wavelength of 1.54 Å with an R-AXIS IV image plate detector using a Rigaku RU300 rotating-anode X-ray generator. Data sets were processed and scaled with d*TREK to 1.95 Å. Model building and refinement of all GmhB structures were conducted through multiple iterations of Coot and REFMAC5 (*33*) until R values and geometry statistics reached suitable ranges (Table 1). Maximal estimated coordinate errors were determined with cross-validated data using SFCHECK within CCP4 Program Suite version 6.1.0 (*34*). All

protein structures were illustrated using PyMOL (DeLano Scientific LLC).

Computational Substrate Docking. The X-ray structure of the GmhB·Ca·P complex (PDB entry 3ESR) was used as a starting model. D-*glycero*-D-*manno*-Heptose 1,7-bisphosphate (HBP) was built, and restraint libraries were generated using the monomer library sketcher program included in the CCP4 program suite (*34*). The resulting HBP model was manually docked into the putative active site of GmhB using Coot such that the cleavable phosphate overlapped with the phosphate from the X-ray structure. The molecular modeling program ZMM (ZMM Software Inc., Flamborough, ON) was used to generate a double-shell model of GmhB centered around the coordinates of the phosphate atom with a 5 Å flexible shell and a 10 Å rigid shell. Energy calculations were performed by the Monte Carlo minimization (MCM) method using the AMBER force field. The HBP substrate molecule was subjected to 2000 random samplings within the double-shell model of GmhB to determine its optimal position, orientation, and conformation within the putative active site. The lowest-energy structure was then further MC-minimized until the energy did not decrease following 2000 minimizations.

D-glycero-D-manno-Heptose 1,7-Bisphosphate Synthesis. D-*glycero*-D-*manno*-Heptose 1,7-bisphosphate (HBP) was synthesized enzymatically from ribose 5-phosphate, D-serine, and ATP in two steps. First, sedoheptulose 7-phosphate (S7P) was synthesized enzymatically as previously described (*16*, *35*). Enzymes were removed using an Amicon Ultra 5 concentrator (3000 rpm, 4 °C, 30 min) to stop the reaction. The filtrate was then combined in a second 5 mL reaction mixture with 25 mM phosphoenolpyruvate (PEP), 30 mM ATP, 10 mM KCl, 20 units of pyruvate kinase (Sigma), and 1 mg of HldE. GmhA (1.5 mg) was used to initiate the reaction. Twenty microliters of sample was removed at 0, 1, 3, and 20 h. The purity of the HBP product was monitored by analytical reverse phase HPLC (Acclaim TM^{20} column, 3 μm, 120 Å, 4.6 mm × 150 mm) using water gradients with 0.05% formic acid as a counterion. Product identification was verified by liquid chromatography−electrospray mass spectrometry (LC−ES-MS) analysis using a QTRAP-LC/MS/MS instrument (Applied Bosystems). After 20 h, the enzymes were again removed using an Amicon Ultra 5 concentrator (3000 rpm, 4 °C, 30 min). The filtrate was applied to a 50 mL Q-Sepharose anion exchange column and the product eluted using a 0 to 1 M ammonium acetate gradient. Fractions were analyzed by LC−MS, and those containing product were combined, lyophilized, washed with water, and lyophilized again. The lyophilized product was stored at −20 °C. The HBP product was confirmed after each step by LC−ES-MS, and the final product was confirmed by ^{13}C and ^{31}P NMR. Both LC−ES-MS and NMR results suggest the presence of minor substrate contaminations in the final product.

GmhB Steady State Kinetic Analysis. The malachite green-phosphomolybdate phosphate detection assay was used in GmhB kinetic studies as previously described (*25*) with the following modifications. The reaction mixture consisted of 20 mM HEPES (pH 8.0), 10 mM $MgCl_2$, 10 mM KCl, and 0.0024 nmol of GmhB, in a total volume of 90 μL. Reactions were initiated with 10 μL of HBP product. Reactions were stopped after 10 min, where the reaction remains in the linear range, using 5% trichloroacetic acid. Twenty microliters of the stopped reaction mixture was diluted to 50 μL with H_2O. Two hundred microliters of malachite green phosphomolybdate reagent was added, and A_{660} was measured after 5 min. Initial rates were fit to eq 1 describing Michaelis−Menten kinetics using Grafit 4 (Erithacus Software, Staines, U.K.).

$$U = k_{cat}E_t[S]/(K_m + [S]) \quad (1)$$

The same procedure was used to determine the concentration of HBP present in each reaction, except 1 mM ATP and 1.5 μg of HldE were added to the reaction mixture and 2−500-fold dilution of the original HBP solution was used to initiate the 60 min reaction.

Secondary Structure Comparison. Circular dichroism spectra of GmhB and GmhB C107A were collected using an AVIV spectropolarimeter equipped with temperature control. Samples were prepared at concentrations of 14 and 22 μM, respectively, in a buffer containing 5 mM HEPES (pH 8.0) and 5% glycerol. The background spectrum of this buffer was subtracted from all measurements. A 1 mm path length quartz cuvette was used for all analysis. Scans were performed from 260 to 200 nm, every 1.0 nm, with equilibration for 30 s at each point, at 25 °C. The spectra are reported as the mean residue molar ellipticity ([θ_n], degrees square centimeters per decimole) as calculated with CDPRO and eq 2:

$$[\theta_n] = [\theta_n]_{observed}(c \times \text{no. of residues})^{-1} \quad (2)$$

where $[\theta_n]_{observed}$ is the measured ellipticity and c is the molar concentration of the protein.

In Vivo Complementation Studies. The low-copy number pBAD30*gmhB* plasmid was used to transform *E. coli* BW25113Δ*gmhB* cells to create a *gmhB*-complemented strain. Positive and negative control strains were created via introduction of pBAD30 into BW25113 and BW25113Δ*gmhA* cells, respectively. Bacteria were cultured overnight at 37 °C in M9 minimal medium with 0.2% arabinose and 100 μg/mL ampicillin. Minimal inhibitory concentrations (MICs) of novobiocin were determined as follows. Overnight cultures, as described above, were diluted to an OD_{600} of 0.11 and further diluted 1:200. Strains were grown at 37 °C in 96-well plates in the presence of varying concentrations of DMSO-dissolved novobiocin (from 2 to 1024 μg/mL). OD_{600} was measured after 24 h to assay growth.

LPS Extraction and Detection. *E. coli* BW25113Δ*gmhA* pBAD30*gmhB* and control strains were grown at 37 °C for 20 h in M9 minimal medium with 0.2% arabinose and 100 μg/mL ampicillin. LPS was extracted from these cells as previously described (*16*, *36*). LPS samples were analyzed by SDS−10% polyacrylamide gel electrophoresis and detected by silver staining as previously described (*16*).

RESULTS

3D Structure of GmhB. The structure of apo GmhB from *E. coli* was determined by SAD phasing and refined to 1.50 Å with R and R_{free} values of 16.0 and 21.0%, respectively. GmhB was crystallized in space group $P2_12_12_1$ with two monomers in the asymmetric unit that superimpose with a rmsd of 0.77 Å. Crystals of GmhB·Ca and GmhB·Ca·P complexes were generated by soaking native GmhB crystals with calcium and/or phosphate. The final structures were refined to 1.95 Å, with R and R_{free} values of 23.4 and 24.9%, and 25.7 and 28.4%, respectively. Only small variations were observed between the two protein monomers in each asymmetric unit. The rmsd values in coordinates for chains A and B in apo, Ca-bound, and Ca·P-bound structures were 0.29, 0.22, and 0.31 Å, respectively.

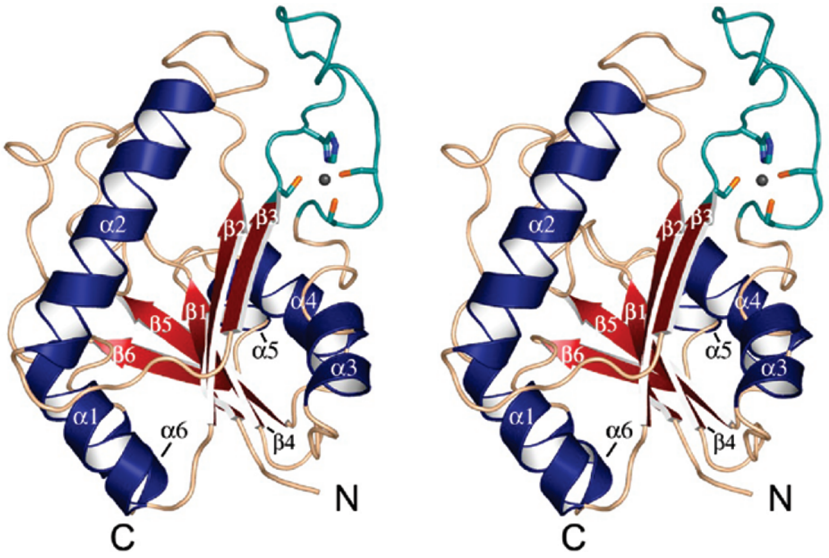

FIGURE 2: Structure of apo GmhB shows as a stereo ribbon diagram of the GmhB crystal structure. Helices (blue) and β-strands (red) are labeled sequentially according to their primary structure. Residues (C92, H93, C107, and C109) within the $\beta3-\alpha3$ loop (cyan) are shown coordinated to a Zn^{2+} ion (gray).

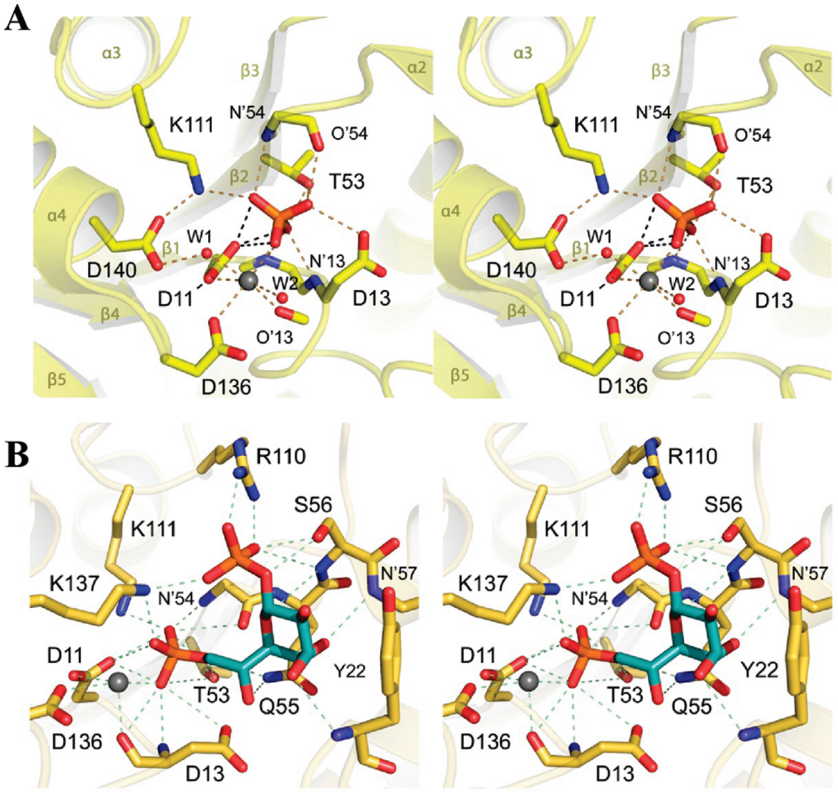

FIGURE 3: GmhB active site. (A) Stereoview of residues and main chain atoms observed to interact with Ca^{2+} (gray) and/or phosphate ions in the GmhB crystal structure. Helices and β-strands are labeled as in Figure 2. Two water molecules (red spheres) that coordinate the divalent metal ion are labeled W1 and W2. Metal coordination, hydrogen bonding, and ionic interactions are indicated with dashed lines. (B) Stereoview of a modeled substrate-bound GmhB structure. The HBP substrate (cyan) was computationally modeled into the active site of GmhB using the phosphate ion coordinates from the GmhB·Ca·P structure as an initial orientation restraint anchor.

The oligomerization state of the protein in solution appears to be monomeric, as suggested by the program PISA and consistent with gel filtration experiments (data not shown).

The structure of GmhB (Figure 2) consists of a single domain with an α/β Rossman fold motif made up of six parallel β-strands ($\beta6$-$\beta5$-$\beta4$-$\beta1$-$\beta2$-$\beta3$) sandwiched between two sets of three α-helices. A search for structural homologues using a DALI server revealed GmhB to have significant homology only to members of the HAD family of proteins (Z score of >10). Two cocrystal structures were determined in the presence of calcium. However, only the GmhB·Ca·P structure is depicted in Figure 3A, as the GmhB·Ca structure provided no additional structural insight. Both structures contained a single Ca^{2+} ion situated at the C-terminal end of $\beta1$, coordinated by the side chains of residues D11 and D136, the main chain of D13, and three solvent molecules (Figure 3A). D11 and D13 fulfill the aspartate

requirement of the conserved DXDX(T/V) motif I observed in the HAD family of phosphatases, while D136 is part of conserved motif III. In the structure of the GmhB·Ca·P complex, the O atoms of the phosphate molecule overlay precisely with four well-ordered water molecules in the structure of the GmhB·Ca complex and the phosphate coordinates the Ca^{2+} ion in place of one of the solvent molecules. Binding of a divalent metal ion appears to stabilize the active site, as *B* factors associated with residues D11, D13, and D136 are all reduced relative to their average apo values in the presence of the Ca^{2+} ion. The bound phosphate interacts with the side chains of residues D11, D13, T53, and K111, and the main chain atoms of R12, D13, and N54, as well as a single contact with the Ca^{2+} ion. T53 corresponds to the requisite S/T from motif II of HAD phosphatases and binds the phosphate moiety as predicted. No major differences are observed in the positions of the main chain atoms between the apo and Ca-bound structures and between the apo and Ca·P-bound structures, with rmsd values of 0.35 and 0.23 Å, respectively. Only relatively minor movements are observed in the side chains of residues in the proximity of the Ca^{2+} ion and phosphate molecule. The complete HBP substrate was modeled into the GmhB·Ca·P structure using the position of the bound phosphate observed in this structure, as shown in Figure 3B. The substrate was readily modeled into the binding pocket without major changes to the position of the bound phosphate or any of the interacting residues.

A single Zn^{2+} ion, as inferred by the observed bond length, is coordinated by the side chains of amino acid residues C92, H93, C107, and C109 and is located at the base of the loop connecting β3 and α3 (Figure 2, cyan-colored loop). As no Zn^{2+} was included in the crystallization buffer, the ion likely plays an important role in structural stability and was probably carried over from purification. The described Zn^{2+} binding pocket has no relationship to any of the known motifs described for this family of proteins, further suggesting its role in secondary structural stability of the protein, rather than catalysis.

GmhB Mutagenesis and Kinetic Characterization. GmhB residues were chosen for analysis on the basis of crystallographic data of the *E. coli* enzyme and its similarity to other members of the HAD superfamily (Figure S1 of the Supporting Information). The predicted catalytic aspartate, D11, and the predicted general acid, D13, were mutated to confirm their predicted essentiality for catalysis on the basis of HAD enzyme precedent and to probe the GmhB mechanism. A predicted catalytic lysine, K111, involved in phosphate binding and stabilization, was also mutated. Finally, to determine the importance of the Zn^{2+} located in the β3−α3 loop, one of the three coordinating cysteines (C107) was selected for mutagenesis.

To monitor GmhB activity directly, we synthesized and purified its substrate, D-*glycero*-D-*manno*-heptose 1,7-bisphosphate (HBP). GmhB activity was measured spectrophotometrically directly through the formation of the inorganic phosphate product, which binds the malachite green−molybdate complex. Using the HBP substrate, activity analysis of purified GmhB wild-type and mutant proteins was conducted (Table 2). D11N, D13N, and K111A mutants appear to be inactive, with no measurable activity observed from either of these mutants (k_{cat} < 0.003 s^{-1}), compared to wild-type activity levels (k_{cat}/K_m = 176 M^{-1} s^{-1}). These results indicate that, as predicted, D11N, D113N, and K111A are all essential for enzyme activity, marking the active site of the protein. Conversely, the Zn^{2+} binding pocket does not appear to be involved directly in activity,

Table 2: GmhB Wild-Type and Mutant Protein Steady State Kinetic Characterization As Determined by the Malachite Green Phosphate Detection Assay

	k_{cat} (s^{-1})	K_m (mM)	k_{cat}/K_m (s^{-1} mM^{-1})
wild type	36 ± 2	0.20 ± 0.03	176
D11N	< 0.003	−	−
D13N	< 0.003	−	−
C107A	17 ± 4	0.7 ± 0.3	26
K111A	< 0.003	−	−

as the creation of a C107A mutant only lowers specificity approximately 5-fold (k_{cat}/K_m = 26 M^{-1} s^{-1}). The role of C107A in structural stability is supported by a significant change to the secondary structure due to the C107A replacement, compared to that of the wild-type enzyme, as observed in the circular dichroism spectra (Figure S2 of the Supporting Information).

In Vitro Genetic Complementation Studies. Deletion of genes encoding most of the enzymes required for ADP-heptose biosynthesis from the *E. coli* chromosome has been shown to abolish the production of full-length LPS (*9*, *15*). However, Kneidinger et al. demonstrated that deleting *gmhB* from the *E. coli* chromosome does not eliminate full-length LPS production (*13*). To confirm this observation and test whether deleting *gmhB* from the chromosome increases susceptibility to novobiocin, *gmhB* was deleted from the *E. coli* BW25113 chromosome and replaced with a kanamycin resistance gene, using the method described by Datsenko et al. (*26*). Figure S3 of the Supporting Information shows that while deleting *gmhA* from the chromosome results in a 10-fold decrease in the MIC of novobiocin, deleting *gmhB* fails to impact the MIC, compared to the parental strain. Therefore, as previously observed, deletion of *gmhB* does not appear to disrupt full-length LPS production to an extent that the outer membrane permeability barrier is compromised (Figure S3). These observations suggest that another protein present in *E. coli* is able to at least partially compensate for the loss in GmhB activity to maintain LPS integrity and precluded further *in vivo* experimentation on the GmhB mutants.

DISCUSSION

On the basis of the protein structural and mutagenic evidence presented here as well as precedent for HAD phosphatases, we propose a mechanism of action for GmhB (Figure 5). The structure of GmhB is similar to those of other phosphatases belonging to the HAD superfamily of enzymes, as demonstrated in Figure 4 (*16*). Members of the HAD superfamily function though nucleophilic attack of the substrate phosphate by a conserved aspartic acid residue, forming a phosphoaspartate enzyme intermediate. The dephosphorylated product is then protonated at the site of attack by a second aspartate serving as a general acid, and the product is released from the active site. In the final step, an activated water molecule attacks the phosphoaspartate intermediate, releasing inorganic phosphate and returning the enzyme to its original form (*21*−*24*). On the basis of the observed structural similarity, D11 is predicted to be the catalytic aspartic acid of GmhB, essential for forming the phosphoenzyme intermediate by attacking the phosphate of HBP at the 7 position. In the GmhB·Ca·P structure (Figure 3), D11 is perfectly situated to carry out this function, and mutagenesis confirmed its essentiality for catalysis of the deprotonation of

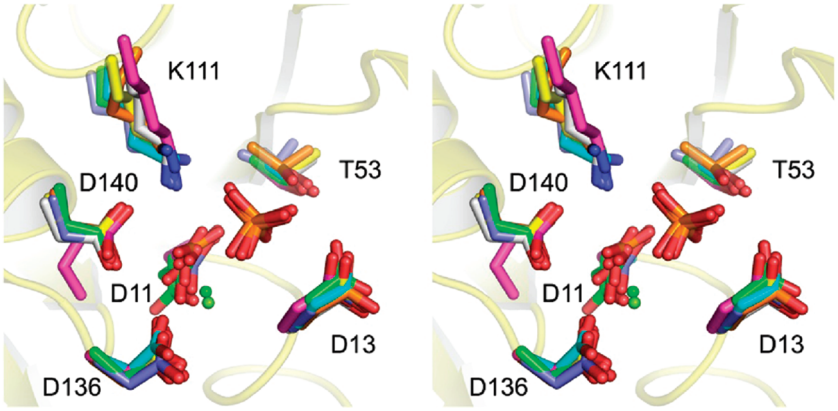

FIGURE 4: Comparison of the active site of HAD family proteins with GmhB. Conserved active site residues from within motifs I and II of HAD family members are shown structurally aligned with analogous residues from GmhB. Residues from different proteins are color coded as follows: phosphoserine phosphatase, green (PDB entry 1F5S); deoxy-D-mannose-octulosonate 8-phosphate phosphatase, cyan (PDB entry 1J8D); β-phosphoglucomutase, purple (PDB entry 1O03); human polynucleotide kinase 3′-phosphatase, white (PDB entry 1YJ5); HAD subclass IIB sugar phosphatase, light blue (PDB entry 1YMQ); phosphonoacetaldehyde hydrolase, orange (PDB entry 2AH5); GmhB, yellow (PDB entry 3ESR). Inorganic phosphate and/or divalent metal ions present in 1F5S, 1YMQ, and 3ESR structures are also shown for the sake of comparison.

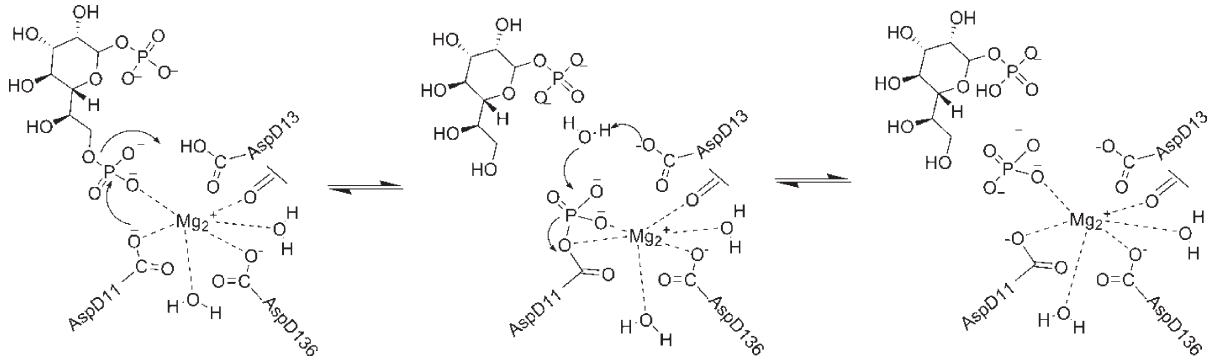

FIGURE 5: GmhB predicted mechanism. The GmhB-catalyzed conversion of D-α,β-D-heptose 1,7-bisphosphate to D-α,β-D-heptose 1-phosphate is predicted to proceed through an aspartylphosphate intermediate.

HBP. D13, in turn, would function as the active site general acid required to protonate the C7 hydroxyl to form the D-*glycero*-D-*manno*-heptose 1-phosphate product and also to activate a water molecule in the final step to initiate inorganic phosphate release. This residue is positioned appropriately in the GmhB·Ca·P structure to carry out these functions and was observed to be necessary for GmhB activity with HBP. On the basis of structural similarity, D13 and D136 would be expected to coordinate the divalent metal ion in the active site and appear to do so, on the basis of the contacts made with the Ca^{2+} present in the active site of the GmhB·Ca and GmhB·Ca·P structures. Similarly, K111 and T53 are predicted to stabilize the phosphoryl group in the active site. Removal of the functional properties of K111 rendered GmhB inactive, suggesting the importance of this residue to catalysis. As well, both K111 and T53 make strong contacts with the phosphate moiety found within the active site, supporting this prediction. Therefore, as outlined in Figure 5, we predict that GmhB converts HBP to H1P via a phosphoaspartate intermediate, utilizing the same mechanism demonstrated for other phosphatases of the HAD superfamily of enzymes.

The GmhB structure also features a Zn^{2+} ion that stabilizes the β3−α3 loop region (Figure 2). Although this feature is not observed in most other HAD family member structures and is not expected to play a role in catalysis, it is absolutely conserved among GmhB homologues and the structurally related histidinol-phosphate phosphatase (HisB). The residues involved in coordinating the Zn^{2+} ion are situated atn either end of this relatively large loop region. A cysteine to alanine substitution at residue 107 resulted in an only slight decrease in GmhB activity, compared to the lack of observable activity when similar analysis was conducted with predicted active site residues (Table 2). Therefore, the function of C107 and its bound Zn^{2+} does not appear to be necessary for catalysis. Although distal from the active site, C107 and C109 are only a couple of residues upstream of the catalytic lysine, K111, and likely confer a measure of stability to this important residue through association with the Zn^{2+} ion. It is not uncommon for enzymes to use a bound Zn^{2+} for the purposes of stability (*37*).

GmhB displays a relatively high degree of sequence similarity (50%) to *E. coli* HisB, a protein involved in histidine biosynthesis. A recent structural study of HisB in complex with a number of ligands has been used as a basis for proposing a unique mechanism for its phosphatase activity (*21*). GmhB and HisB are suggested to be byproducts of a gene duplication event of an ancestral HAD family phosphatase with comparatively flexible substrate specificity (*38*). This would suggest that while GmhB and HisB differ in their selection of substrates, they may still share similar modes of catalysis. Despite the evidence from Brilli et al. that GmhB and HisB are encoded by paralogous genes (*38*), key structural characteristics of the proposed HisB mechanism are notably absent from the structures of GmhB reported in this study. In both reported metal ion-bound structures, only a single metal binding site was observed in the active site cleft of GmhB despite rigorous inspection of the electron density.

Additionally, the key residue (F23) involved in coordinating the second metal ion as described in the HisB mechanism is part of a three-residue insertion in the loop connecting β1 and α1 that is universally absent in GmhB (Figure S1). Given these significant differences, it would appear that GmhB carries out its function in a manner that is typical of that described for HAD family phosphatases and does not mimic the distinct mechanism described for HisB.

GmhB catalyzes a reaction essential to the biosynthesis of ADP-heptose. In the struggle to identify new methods for combatting antibiotic resistance, this molecule represents one of the known targets that remains untapped. The appeal to target ADP-heptose biosynthesis is twofold. (1) The outer core OS and O antigen of Gram-negative bacteria are essential for virulence, and (2) disruption of the OM rescues the effectiveness of numerous clinically useful antibiotics. Unlike the other three enzymes in the ADP-heptose biosynthetic pathway, the deletion of *gmhB* does not induce susceptibility to these antibiotics, specifically novobiocin, nor does it sufficiently truncate LPS in *E. coli*. This finding suggests that one or more other phosphatases may be present in the *E. coli* genome that can compensate for the lack of GmhB activity and corroborates the findings of Kneidinger et al. (*13*). It should be noted, though, that GmhB has been deemed an essential enzyme for OM heptose biosynthesis in other clinically relevant Gram-negative species such as the causative agent of meningococcal meningitis, *Neisseria meningitidis* (*39*), illustrating that not all species necessarily have redundant phosphatases. The dispensability of GmhB has yet to be analyzed in other pathogens, suggesting that while not in *E. coli*, GmhB remains a target for antibiotic adjuvants in Gram-negative pathogens. In fact, such differences could be highly exploitable in the development of species specific antibiotic adjuvant combinations where normal microbial flora could be excluded from killing (e.g., *E. coli*), while selectively targeting pathogens (e.g., *N. meningitidis*).

ACKNOWLEDGMENT

Structural data were collected at the National Synchrotron Light Source, Brookhaven National Laboratory, at beamlines X8C and X12C. We thank Leonid Flaks, Alexei Soares, and Robert Sweet for their technical assistance with structural data collection and Raquel Epand for her assistance with circular dichroism experiments.

SUPPORTING INFORMATION AVAILABLE

A table listing the sequence of DNA primers used to generate *gmhB* point mutations, a structure-based sequence alignment of GmhB and HisB genes from various pathogens, circular dichroism spectra of GmhB and GmhB C107A, and *in vivo* analysis of GmhB essentiality in *E. coli*. This material is available free of charge via the Internet at http://pubs.acs.org.

REFERENCES

1. Nikaido, H. (2001) Preventing drug access to targets: Cell surface permeability barriers and active efflux in bacteria. *Semin. Cell Dev. Biol. 12*, 215–223.
2. Yethon, J. A., and Whitfield, C. (2001) Lipopolysaccharide as a target for the development of novel therapeutics in Gram-negative bacteria. *Curr. Drug Targets Infect. Disord. 1*, 91–106.
3. Poole, K. (2002) Outer membranes and efflux: The path to multidrug resistance in Gram-negative bacteria. *Curr. Pharm. Biotechnol. 3*, 77–98.
4. Raetz, C. R., and Whitfield, C. (2002) Lipopolysaccharide endotoxins. *Annu. Rev. Biochem. 71*, 635–700.
5. Nikaido, H., and Vaara, M. (1985) Molecular basis of bacterial outer membrane permeability. *Microbiol. Rev. 49*, 1–32.
6. Nikaido, H. (2003) Molecular basis of bacterial outer membrane permeability revisited. *Microbiol. Mol. Biol. Rev. 67*, 593–656.
7. Mdluli, K. E., Witte, P. R., Kline, T., Barb, A. W., Erwin, A. L., Mansfield, B. E., McClerren, A. L., Pirrung, M. C., Tumey, L. N., Warrener, P., Raetz, C. R., and Stover, C. K. (2006) Molecular validation of LpxC as an antibacterial drug target in *Pseudomonas aeruginosa*. *Antimicrob. Agents Chemother. 50*, 2178–2184.
8. Barb, A. W., McClerren, A. L., Snehelatha, K., Reynolds, C. M., Zhou, P., and Raetz, C. R. (2007) Inhibition of lipid A biosynthesis as the primary mechanism of CHIR-090 antibiotic activity in *Escherichia coli*. *Biochemistry 46*, 3793–3802.
9. McArthur, F., Andersson, C. E., Loutet, S., Mowbray, S. L., and Valvano, M. A. (2005) Functional analysis of the glycero-manno-heptose 7-phosphate kinase domain from the bifunctional HldE protein, which is involved in ADP-L-glycero-D-manno-heptose biosynthesis. *J. Bacteriol. 187*, 5292–5300.
10. Tamaki, S., Sato, T., and Matsuhashi, M. (1971) Role of lipopolysaccharides in antibiotic resistance and bacteriophage adsorption of *Escherichia coli* K-12. *J. Bacteriol. 105*, 968–975.
11. Valvano, M. A., Messner, P., and Kosma, P. (2002) Novel pathways for biosynthesis of nucleotide-activated glycero-manno-heptose precursors of bacterial glycoproteins and cell surface polysaccharides. *Microbiology 148*, 1979–1989.
12. Kneidinger, B., Graninger, M., Puchberger, M., Kosma, P., and Messner, P. (2001) Biosynthesis of nucleotide-activated D-glycero-D-manno-heptose. *J. Biol. Chem. 276*, 20935–20944.
13. Kneidinger, B., Marolda, C., Graninger, M., Zamyatina, A., McArthur, F., Kosma, P., Valvano, M. A., and Messner, P. (2002) Biosynthesis pathway of ADP-L-glycero-β-D-manno-heptose in *Escherichia coli*. *J. Bacteriol. 184*, 363–369.
14. Eidels, L., and Osborn, M. J. (1974) Phosphoheptose isomerase, first enzyme in the biosynthesis of aldoheptose in *Salmonella typhimurium*. *J. Biol. Chem. 249*, 5642–5648.
15. Brooke, J. S., and Valvano, M. A. (1996) Molecular cloning of the *Haemophilus influenzae* gmhA (lpcA) gene encoding a phosphoheptose isomerase required for lipooligosaccharide biosynthesis. *J. Bacteriol. 178*, 3339–3341.
16. Taylor, P. L., Blakely, K. M., de Leon, G. P., Walker, J. R., McArthur, F., Evdokimova, E., Zhang, K., Valvano, M. A., Wright, G. D., and Junop, M. S. (2008) Structure and function of sedoheptulose-7-phosphate isomerase, a critical enzyme for lipopolysaccharide biosynthesis and a target for antibiotic adjuvants. *J. Biol. Chem. 283*, 2835–2845.
17. Valvano, M. A., Marolda, C. L., Bittner, M., Glaskin-Clay, M., Simon, T. L., and Klena, J. D. (2000) The rfaE gene from *Escherichia coli* encodes a bifunctional protein involved in biosynthesis of the lipopolysaccharide core precursor ADP-L-glycero-D-manno-heptose. *J. Bacteriol. 182*, 488–497.
18. Loutet, S. A., Flannagan, R. S., Kooi, C., Sokol, P. A., and Valvano, M. A. (2006) A complete lipopolysaccharide inner core oligosaccharide is required for resistance of *Burkholderia cenocepacia* to antimicrobial peptides and bacterial survival in vivo. *J. Bacteriol. 188*, 2073–2080.
19. Sirisena, D. M., MacLachlan, P. R., Liu, S. L., Hessel, A., and Sanderson, K. E. (1994) Molecular analysis of the rfaD gene, for heptose synthesis, and the rfaF gene, for heptose transfer, in lipopolysaccharide synthesis in *Salmonella typhimurium*. *J. Bacteriol. 176*, 2379–2385.
20. Morrison, J. P., and Tanner, M. E. (2007) A two-base mechanism for *Escherichia coli* ADP-L-glycero-D-manno-heptose 6-epimerase. *Biochemistry 46*, 3916–3924.
21. Rangarajan, E. S., Proteau, A., Wagner, J., Hung, M. N., Matte, A., and Cygler, M. (2006) Structural snapshots of *Escherichia coli* histidinol phosphate phosphatase along the reaction pathway. *J. Biol. Chem. 281*, 37930–37941.
22. Lahiri, S. D., Zhang, G., Dunaway-Mariano, D., and Allen, K. N. (2003) The pentacovalent phosphorus intermediate of a phosphoryl transfer reaction. *Science 299*, 2067–2071.
23. Allen, K. N., and Dunaway-Mariano, D. (2004) Phosphoryl group transfer: Evolution of a catalytic scaffold. *Trends Biochem. Sci. 29*, 495–503.
24. Lu, Z., Dunaway-Mariano, D., and Allen, K. N. (2008) The catalytic scaffold of the haloalkanoic acid dehalogenase enzyme superfamily acts as a mold for the trigonal bipyramidal transition state. *Proc. Natl. Acad. Sci. U.S.A. 105*, 5687–5692.
25. De Leon, G. P., Elowe, N. H., Koteva, K. P., Valvano, M. A., and Wright, G. D. (2006) An in vitro screen of bacterial lipopolysaccharide biosynthetic enzymes identifies an inhibitor of ADP-heptose biosynthesis. *Chem. Biol. 13*, 437–441.
26. Datsenko, K. A., and Wanner, B. L. (2000) One-step inactivation of chromosomal genes in *Escherichia coli* K-12 using PCR products. *Proc. Natl. Acad. Sci. U.S.A. 97*, 6640–6645.

27. Hendrickson, W. A., Horton, J. R., and LeMaster, D. M. (1990) Selenomethionyl proteins produced for analysis by multiwavelength anomalous diffraction (MAD): A vehicle for direct determination of three-dimensional structure. *EMBO J. 9*, 1665–1672.
28. Pflugrath, J. W. (1999) The finer things in X-ray diffraction data collection. *Acta Crystallogr. D55*, 1718–1725.
29. Adams, P. D., Grosse-Kunstleve, R. W., Hung, L. W., Ioerger, T. R., McCoy, A. J., Moriarty, N. W., Read, R. J., Sacchettini, J. C., Sauter, N. K., and Terwilliger, T. C. (2002) PHENIX: Building new software for automated crystallographic structure determination. *Acta Crystallogr. D58*, 1948–1954.
30. Brunger, A. T., Adams, P. D., Clore, G. M., DeLano, W. L., Gros, P., Grosse-Kunstleve, R. W., Jiang, J. S., Kuszewski, J., Nilges, M., Pannu, N. S., Read, R. J., Rice, L. M., Simonson, T., and Warren, G. L. (1998) Crystallography & NMR system: A new software suite for macromolecular structure determination. *Acta Crystallogr. D54*, 905–921.
31. Emsley, P., and Cowtan, K. (2004) Coot: Model-building tools for molecular graphics. *Acta Crystallogr. D60*, 2126–2132.
32. McCoy, A. J., Grosse-Kunstleve, R. W., Adams, P. D., Winn, M. D., Storoni, L. C., and Read, R. J. (2007) Phaser crystallographic software. *J. Appl. Crystallogr. 40*, 658–674.
33. Murshudov, G., (1996) in Abstracts of the Proceedings of the Daresbury Study Weekend, pp 93−104, SERC, Daresbury Laboratory, Warrington, U.K.
34. Collaborative Computational Project, Number 4 (1994) The CCP4 suite: Programs for protein crystallography. *Acta Crystallogr. D50*, 760–763.
35. Lee, S., Kirschning, A., Muller, M., Way, C., and Floss, H. G. (1999) Enzymatic synthesis of [7-^{14}C,7-^{3}H] and [1-^{13}C]sedoheptulose 7-phosphate and [1-^{13}C]ido-heptulose 7-phosphate. *J. Mol. Catal. B: Enzym. 6*, 369–377.
36. Marolda, C. L., Lahiry, P., Vines, E., Saldias, S., and Valvano, M. A. (2006) Micromethods for the characterization of lipid A-core and O-antigen lipopolysaccharide. *Methods Mol. Biol. 347*, 237–252.
37. Berg, J. M., and Godwin, H. A. (1997) Lessons from zinc-binding peptides. *Annu. Rev. Biophys. Biomol. Struct. 26*, 357–371.
38. Brilli, M., and Fani, R. (2004) Molecular evolution of hisB genes. *J. Mol. Evol. 58*, 225–237.
39. Shih, G. C., Kahler, C. M., Carlson, R. W., Rahman, M. M., and Stephens, D. S. (2001) gmhX, a novel gene required for the incorporation of L-glycero-D-manno-heptose into lipooligosaccharide in *Neisseria meningitidis*. *Microbiology 147*, 2367–2377.